Z. Phys. C – Particles and Fields 48, 393–400 (1990)

Zeitschrift für Physik C Particles and Fields
© Springer-Verlag 1990

Measurement of two photon production of $\rho^0\omega$

JADE Collaboration

A. Wegner[2], J. Olsson[1], J. Allison[5], K. Ambrus[3a], R.J. Barlow[5], W. Bartel[1], S. Bethke[3], C.K. Bowdery[4], S.L. Cartwright[7b], J. Chrin[5], D. Clarke[7], A. Dieckmann[3], I.P. Duerdoth[5], G. Eckerlin[3], E. Elsen[3c], R. Felst[1], A.J. Finch[4], F. Foster[4], T. Greenshaw[2], J. Hagemann[2d], D. Haidt[1], J. Heintze[3], G. Heinzelmann[2], K.H. Hellenbrand[3e], P. Hill[6c], G. Hughes[4], H. Kado[1f], K. Kawagoe[8], T. Kawamoto[8], C. Kleinwort[2d], G. Knies[1], S. Komamiya[3g], H. Krehbiel[1], J. v. Krogh[3], M. Kuhlen[2h], F.K. Loebinger[5], A.A. Macbeth[5], N. Magnussen[1i], R. Marshall[7], R. Meinke[1], R.P. Middleton[7], P.G. Murphy[5], B. Naroska[2], J.M. Nye[4j], F. Ould-Saada[2], D. Pitzl[2k], R. Ramcke[1l], H. Rieseberg[3], D. Schmidt[1i], L. Smolik[3c], U. Schneekloth[2c], J.A.J. Skard[6m], J. Spitzer[3], P. Steffen[1], K. Stephens[5], T. Takeshita[8], A. Wagner[3], I.W. Walker[4], G. Weber[2], M. Zimmer[3c], G.T. Zorn[6]

[1] Deutsches Elektronen-Synchrotron DESY, D-2000 Hamburg, Federal Republic of Germany
[2] II. Institut für Experimentalphysik der Universität Hamburg, D-2000-Hamburg, Federal Republic of Germany
[3] Physikalisches Institut der Universität Heidelberg, D-6900 Heidelberg, Federal Republic of Germany
[4] University of Lancaster, Lancaster, England
[5] University of Manchester, Manchester, England
[6] University of Maryland, College Park, MD, USA
[7] Rutherford Appleton Laboratory, Chilton, Didcot, England
[8] International Center for Elementary Particle Physics, University of Tokyo, Tokyo , Japan

Received 2 July 1990

Abstract. The reaction $\gamma\gamma\to\pi^+\pi^-\pi^+\pi^-\pi^0$ has been studied using the JADE detector at PETRA. The cross sections for $\gamma\gamma\to\omega\pi^+\pi^-$ and for $\gamma\gamma\to\omega\rho^0$ are given. We observe no peak in these cross sections in the region $W_{\gamma\gamma}=1.9$–2.0 GeV.

Introduction

In 1980 the TASSO collaboration [1] observed a large enhancement in the threshold region of the cross section $\sigma_{\gamma\gamma\to\rho^0\rho^0}$ and this result has since been confirmed by other groups [2–5]. This threshold enhancement is in disagreement with naive Vector Dominance predictions [1]. Simple resonance explanations must also be ruled out, since the measurement of the cross section for the charge conjugate reaction $\gamma\gamma\to\rho^+\rho^-$ [6] showed this process to be strongly suppressed. If the enhancement of the cross section $\gamma\gamma\to\rho^0\rho^0$ is due to the production of a simple resonance, isospin invariance would predict a relation 2/1 or 1/2 for the ratio $\sigma_{\gamma\gamma\to\rho^+\rho^-}/\sigma_{\gamma\gamma\to\rho^0\rho^0}$, for isospin 0 or 2 respectively. However the resonance interpretation can be maintained by invoking a model where states with different isospins interfere.

In the $q\bar{q}q\bar{q}$ model of Achasov et al. [7, 8] and Li and Liu [9, 10] the measured cross sections are explained by the production of intermediate $q\bar{q}q\bar{q}$ resonances. In this model three $q\bar{q}q\bar{q}$ states of the same mass, two with isospin 0 and one with isospin 2, contribute to the cross sections $\sigma_{\gamma\gamma\to\rho^0\rho^0}$ and $\sigma_{\gamma\gamma\to\rho^+\rho^-}$. Constructive interference of these states produces a high cross section in the case of $\sigma_{\gamma\gamma\to\rho^0\rho^0}$, while destructive interference leads to the suppression of $\sigma_{\gamma\gamma\to\rho^+\rho^-}$.

A more conservative approach, which is also able to explain the measured cross sections, is the t-channel factorization model of Alexander, Levy, Williams and Maor [11–13]. In this model, factorization is assumed in the t-channel and the cross section $\sigma_{\gamma\gamma\to\rho\rho}$ is inferred from photoproduction data $\sigma_{\gamma N\to\rho N}$ and from nucleon-nucleon cross sections. The enhancement in $\sigma_{\gamma\gamma\to\rho^0\rho^0}$ and the suppression of $\sigma_{\gamma\gamma\to\rho^+\rho^-}$ are both explained in this approach.

[a] Now at MBB, D-8000 Munich, Federal Republic of Germany
[b] Now at Sheffield University, Sheffield, UK
[c] Now at DESY, D-2000 Hamburg, Federal Republic of Germany
[d] Now at CERN, CH-Geneva, Switzerland
[e] Now at Universität des Saarlandes, D-6600 Saarbrücken, Federal Republic of Germany
[f] Now at Bayer AG, D-2212 Brunsbüttel, Federal Republic of Germany
[g] Now at SLAC, California, USA
[h] Now at CALTECH, California, USA
[i] Universität-Gesamthochschule Wuppertal, D-5600 Wuppertal, Federal Republic of Germany
[j] Now at ESTEC, Noordwijk, The Netherlands
[k] Now at Santa Cruz, California, USA
[l] Now at Ramcke Datentechnik GmbH, D-2000 Hamburg, Federal Republic of Germany
[m] Now at ST Systems Corporation, Lanham, MD, USA

Both models also make predictions about the two photon production of other vector meson pairs, i.e. the reactions $\gamma\gamma \to VV'$ where VV' are $\rho^0\rho^0$, $\rho^+\rho^-$, $\omega\rho^0$, $\omega\omega$, $\omega\phi$, $\rho^0\phi$, $\phi\phi$, $K^{*0}\overline{K^{*0}}$ and $K^{*+}K^{*-}$. A measurement of these processes can be used to test the models.

In this paper we report on a measurement of the $\gamma\gamma$ reaction:

$$e^+e^- \to e^+e^-\omega\rho^0 \to e^+e^-2\pi^+2\pi^-\pi^0. \quad (1)$$

The electrons are in general scattered at small angles and remain in the beam pipe (no-tag events). Therefore the final state consists of four charged pions with low momentum and two photons with low energy.

The measurement was performed with the JADE detector at the PETRA e^+e^- storage ring. The integrated luminosity was 224 pb^{-1}, obtained at an average beam energy of 18 GeV.

Detector

The JADE detector has been described in detail elsewhere [14]. Here we mention only those features of the detector that were pertinent to the present analysis. Of particular importance was the ability to trigger efficiently on final states with only a few tracks and with low visible energy and to detect and measure low energy photons, typically of a few hundred MeV or less.

Photons were detected in an array of 2712 lead glass Čerenkov counters located behind the central jet chamber and the coil. A barrel section and two end cap sections furnished a solid angle coverage of 90%, with the barrel part subtending $|\cos\theta| < 0.82$ and the endcap parts covering $0.89 < |\cos\theta| < 0.97$, where θ is the polar angle with respect to the beam axis. The barrel counters were arranged in 84 rows parallel to the beam axis, each with 30 counters, while the endcaps consisted of 96 counters each, arranged in 4 quadrants of 24 counters. The practical lower limit for detectable photon energies was $\sim$40 MeV determined by the readout threshold of the lead glass counter electronics. The energy resolution varied between 33% and 13% for photon energies from 50 to 400 MeV, while the angular resolution was $\sigma_\phi \sim \sigma_\theta \sim 25$ mrad at these energies.

The inner detector or "jet chamber" was a cylindrical drift chamber with wires parallel to the beam axis. It was used for charged particle detection and together with the magnetic field of 0.48 T provided momentum determination. The lower limit for the measurable pion momentum of 30 MeV/c was determined by the efficiency of the charged track pattern recognition program for the inner detector. The error of the measurement in the momentum region of interest (a few hundred MeV/c) was dominated by multiple scattering in the material of the inner detector and was 4%. The inner detector also aided particle identification via dE/dx measurements, made at up to 48 points along the particle's track. The time of flight (TOF) counters consisted of 42 sheets of plastic scintillator mounted just outside the inner detector. They played a major role in the trigger system.

The events used in this analysis were triggered in two steps. The first step (T1) was based on the signals of the TOF counters and the barrel lead glass counters. If the energy sum of the 6 barrel counter rows behind a fired TOF counter was above the threshold of 80 MeV a so-called TOF *barrel group* (TBG) was set. The T1 trigger conditions were:

a) Two fired TOF counters nearly coplanar with the beam (coplanarity width of one TOF counter) were required. A maximum of six fired TOF counters was allowed.

b) For the second T1 trigger the same conditions as above were used but with a coplanarity width of three TOF counters and a maximum number of four fired TOF counters.

c) Two coplanar TBG elements with a coplanarity width of two TOF counters were required.

d) Two TBG elements with a minimum distance of three TOF counters and a maximum of six fired TOF counters were required.

If at least one of the T1 conditions was fulfilled the trigger decision was postponed to the next step. This, T2, was a charged track trigger which compared the hit sense wires of the jet chamber with given patterns and hence identified tracks. At least two tracks were required in this trigger step. If the T1 conditions a)–c) were fulfilled these tracks were required to be coplanar with the beam.

Event selection

The ρ^0 meson decays exclusively into $\pi^+\pi^-$ and the ω meson mainly into $\pi^+\pi^-\pi^0$ (with a branching ratio of 89%). Therefore, in a first step, events with exactly four charged tracks and two photons were selected with the following criteria:

- Charged tracks were required to have at least 8 measured points in the inner detector and to have a momentum greater than 100 MeV/c. They also had to originate in a fiducial cylinder around the interaction point with radius 20 mm and length $\pm$200 mm. These criteria were not applied to tracks obviously coming from nuclear interactions in the outer wall of the pressure vessel or the coil (backscattering) or tracks from photon conversions. Events containing such tracks, provided they satisfied all other criteria, were kept in the sample under study.
- A photon was defined to be either a reconstructed e^+e^- pair from a conversion or an energy cluster in the lead glass array to which no charged tracks could be associated. Clusters consisting of only one lead glass counter were required to have at least 40 MeV reconstructed photon energy. Since photons in the endcap lead glass counter had bad angular and energy resolution, events with any such photon were rejected.

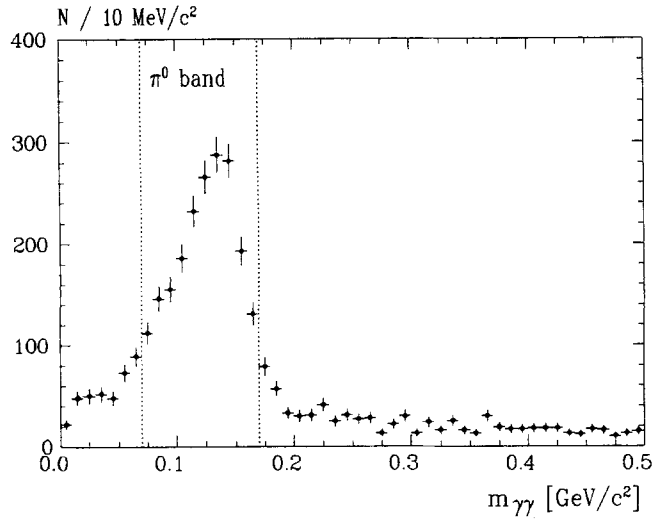

Fig. 1. Invariant $\gamma\gamma$ mass

Due to hard scattering of charged particles in the outer wall of the pressure vessel or the coil the association of a track to a lead glass cluster sometimes failed and the cluster was misinterpreted as being due to a photon. Another source of fake photons were clusters produced by secondaries generated in nuclear interactions by charged pions in the outer wall of the pressure vessel or the coil. Since most of the fake photons were related to lead glass clusters near the position at which the track hit the lead glass, the requirement that the angular separation of tracks and clusters (assuming they come from the interaction point) was greater than 18° rejected most of these spurious events.

A total of 15374 events passed these criteria. Further cuts were applied to reduce background and enrich the sample with $2\pi^+ 2\pi^- \pi^0$ events containing an ω meson:

- It was required that the charged tracks had a dE/dx measurement consistent with the pion hypothesis ($\chi^2 < 9 \cdot \sigma^2_{dE/dx}$).
- To reject beam-gas events the reconstructed common z-vertex of the four tracks had to be within ± 50 mm of the interaction point.
- The large cross section of the reaction $\gamma\gamma \to \rho^0\rho^0 \to 2\pi^+ 2\pi^-$ together with additional noise in the lead glass caused a considerable contamination of our sample by events of the kind $\gamma\gamma \to 2\pi^+ 2\pi^-$. In order to suppress this background the transverse momentum squared of the four charged pions was required to be larger than 0.005 (GeV/c)^2.
- After the above cuts the invariant $\gamma\gamma$ mass exhibits a clear π^0 signal (Fig. 1). All events with an invariant $\gamma\gamma$ mass between 0.07 GeV/c^2 and 0.18 GeV/c^2, as indicated by the π^0 band in Fig. 1, were accepted and a constrained 1 C-fit to the π^0 mass was performed.
- To reject background from non-exclusive events (i.e. events with additional, undetected particles) and to restrict the range of the absolute value of the virtual photon 4-momenta squared (Q^2) to small ("quasi real") values, only events with total transverse momentum squared ($p_\perp^2$) of less than 0.01 (GeV/c)^2 were accepted. A constrained 2 C-fit to the $p_\perp = 0$ hypothesis improved the mass resolution and facilitated the identification of the ω meson.

A total of 539 events remained after these cuts. There are four ways of choosing the decay products of the ω meson, $\pi^+\pi^-\pi^0$, from the five pions. To reduce combinatorial and other backgrounds, the kinematic properties of the three body decay of the ω meson were exploited by means of the Dalitz plot. The Dalitz plot for the ω meson has its maximum density in the centre and so only those $\pi^+\pi^-\pi^0$ combinations in the inner 65% of the Dalitz plot (containing 89% of the ω signal) were accepted. Figure 2a shows the distribution of the $\pi^+\pi^-\pi^0$ combination in the Dalitz plot. In Fig. 2b the corresponding invariant $\pi^+\pi^-\pi^0$ mass spectra for all combinations and for the combinations at the border of the Dalitz plot are shown.

The events with at least one $\pi^+\pi^-\pi^0$ combination in the centre of the Daltz plot were visually inspected with help of a graphics display program and some background events, mainly those with unrecognized conver-

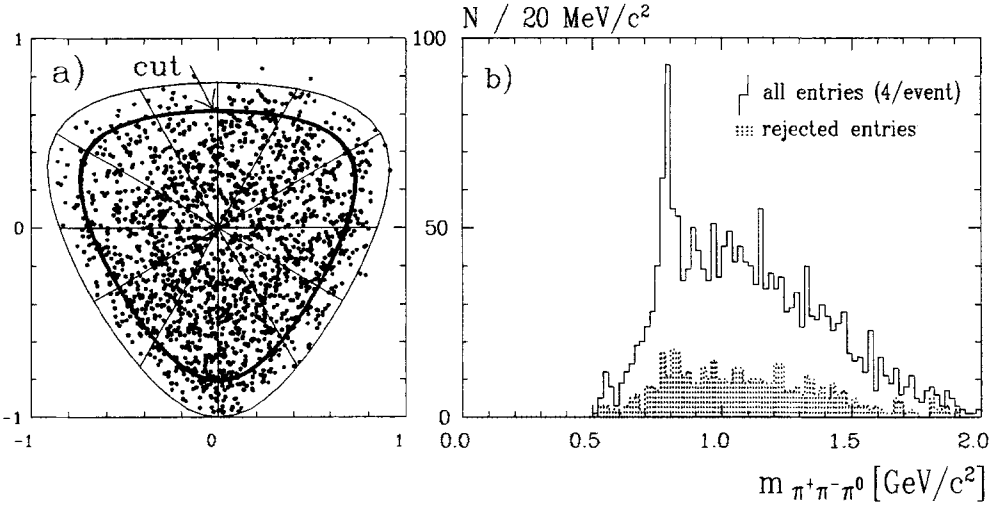

Fig. 2. a Distribution of $\pi^+\pi^-\pi^0$ combinations in the Dalitz plot. **b** $\pi^+\pi^-\pi^0$ mass spectra for all combinations and for $\pi^+\pi^-\pi^0$ combinations at the border of the Dalitz plot (shaded)

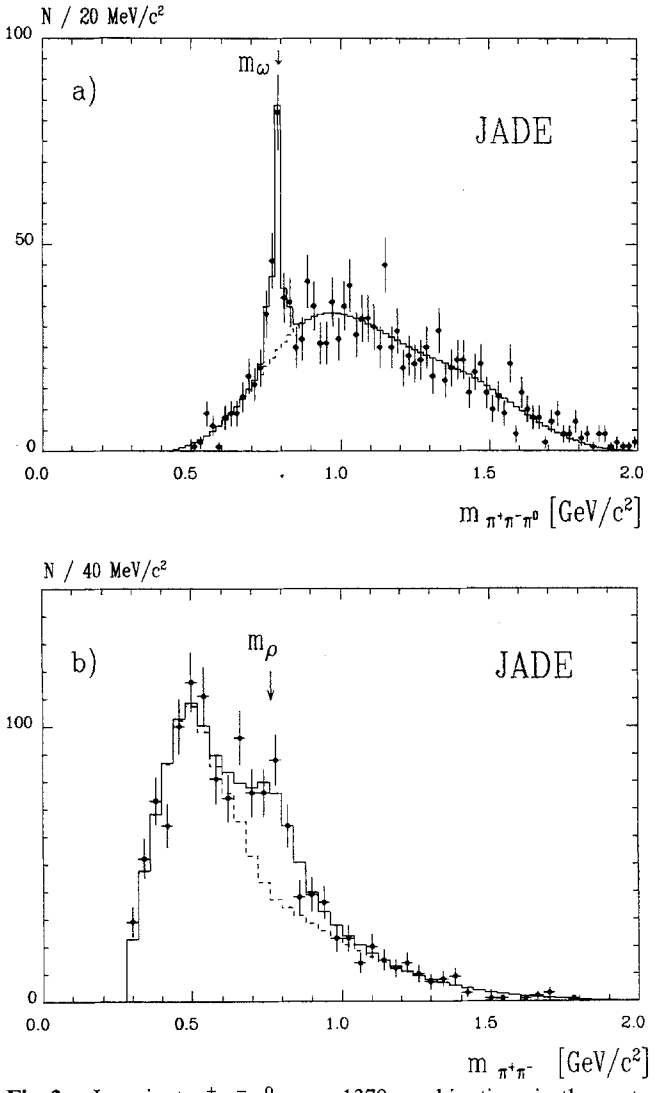

Fig. 3. a Invariant $\pi^+\pi^-\pi^0$ mass, 1370 combinations in the centre of the Dalitz plot. **b** Invariant $\pi^+\pi^-$ mass, only those combinations recoiling against the $\pi^+\pi^-\pi^0$ combinations in **a** are entered. Also shown are fits to Monte Carlo processes (see text)

sions, were rejected. After this selection, 465 events in the $W_{\gamma\gamma}$ (the total CMS energy of the $\gamma\gamma$ system) range from 1.2 GeV to 3.0 GeV with 1370 $\pi^+\pi^-\pi^0$ combinations in the centre of the Dalitz plot remained. In Fig. 3a, the invariant mass spectrum of these combinations is plotted. A clear ω signal can be seen. The recoiling $\pi^+\pi^-$ masses are shown in Fig. 3b. The $\pi^+\pi^-$ mass spectrum exhibits an enhancement in the ρ^0 region.

Monte Carlo simulation

The detector acceptance was calculated using Monte Carlo generated events. The simulation procedure started by generating the 4-momenta of the $\gamma\gamma$ system using the program of Ref. 15. This program performed an integration of the luminosity function, in the formulation of Bonneau et al. [16]. Only the transverse-transverse polarization component (Eq. (29d) in [16]) was considered. A cross section $\sigma_{\gamma\gamma}$ (σ_{TT} in [16]) independent of $W_{\gamma\gamma}$ was used. To account for the Q^2 dependence of $\sigma_{\gamma\gamma}$, both virtual photons were multiplied by a ρ formfactor, $1/(1+Q^2/M_\rho^2)^2$, in the integration of the luminosity function. In the next step a phase space decay of the invariant mass $W_{\gamma\gamma}$ into $\omega\rho^0$ using the program SAGE [17] was performed. To describe the mass dependence of the width of the broad ρ^0 meson the parameterization of [18] was used:

$$\Gamma(m)=\Gamma(m_0)\left(\frac{p}{p_0}\right)^{2j+1}\left(\frac{2p_0^2}{p_0^2+p^2}\right) \qquad \Gamma(m_0)=153\ \text{MeV}$$

Here $\Gamma(m_0)$ is the nominal width of the ρ^0 meson, p_0 is the momentum of the decay products at the nominal ρ mass and p is the corresponding momentum at the actual $\pi^+\pi^-$ mass. The spin is $j=1$ for the ρ^0 meson.

Subsequently, the ω meson was allowed to decay into three pions with an appropriate matrix element while the ρ^0 meson decayed according to two body phase space into $\pi^+\pi^-$. The 4-vector events generated in this way were then passed through the JADE detector simulation program, which included a full shower simulation [19] for photons and electrons. The Čerenkov radiation response of the leadglass (SF5 and SF6) was accurately simulated, including the wavelength dependence of the photocathode sensitivity and the light transmission in lead glass and light guide material. Finally, the simulated events were subjected to the same selection cuts as the real events.

Detection efficiency

In the determination of the detector acceptance, in particular of the trigger efficiency, corrections were made for the following effects:

- The threshold behaviour of the TBG trigger elements as a function of the deposited energy or the pion momentum was important, since most triggered events of reaction (1) were close to the threshold. Efficiency curves of the TBG trigger elements as a function of deposited lead glass energy (for photons) or of the pion momentum (for pions setting the TBG elements) were obtained using events triggered in other, independent ways. These curves were used in the Monte Carlo simulation.
- Spurious background hits in the TOF counters led to a reduction of the trigger efficiency since three of the four triggers included a veto against too many fired TOF counters. The rate for this effect was inferred from data and included in the Monte Carlo simulation.
- The loss of events due to nuclear interactions of charged pions in the beampipe or in the material in front of the drift chambers was corrected for using measured cross sections of pions in aluminium [20].

In the first selection step, only events with exactly two photons were accepted and so any additional photon from tracks interacting in the outer tank wall or the coil or fake photons due to noise in the lead glass caused a loss of good events. To determine the extent of this loss, the leakage of $\gamma\gamma\to\pi^+\pi^-\pi^+\pi^-$ events, which are

quite similar in topology to the state $\pi^+\pi^-\pi^+\pi^-\pi^0$, into 4 track 1, 2, and 3 gamma samples, was measured. The $\gamma\gamma\to\pi^+\pi^-\pi^+\pi^-$ events were identified by means of the peak in the distribution of the transverse momentum of the four charged pions [21]. From the number of events in these peaks relative to the peak in the 4 track 0 gamma data sample a correction factor of 1.28 was deduced.

The most serious background was caused by the contamination by events from the reactions $\gamma\gamma\to\omega\omega$ and $\gamma\gamma\to\omega\pi^+\pi^-\pi^0$ with two undetected photons, since these events contain completely reconstructed ω mesons. The cross sections for both processes have been measured by the ARGUS collaboration [22] and these measurements were used to compute the background by means of a Monte Carlo simulation. It was found that 189 ± 90 entries in the $\pi^+\pi^-\pi^0$ mass spectra with 18 ± 9 reconstructed ω mesons were expected in our sample.

The main contribution to the systematic error of the measurement of the cross section $\sigma_{\gamma\gamma\to\omega\rho^0}$ came from uncertainties in the detector simulation ($\approx12\%$) and in the event selection (10%), the e^+e^- luminosity determination (3%) and the determination of the detection efficiency (4%). The systematic errors of the ARGUS measurements of the reactions $\gamma\gamma\to\omega\omega$ and $\gamma\gamma\to\omega\pi^+\pi^-\pi^0$ gave an additional systematic uncertainty of 4% in the background subtraction. Finally minor systematic contributions came from the VDM (photon form factor parameterization) and from the simulation of the $\gamma\gamma$ luminosity function. After adding all values in quadrature the systematic error was estimated to be 17%.

Cross sections

The goal of the analysis was to measure the cross section $\sigma_{\gamma\gamma\to\omega\rho^0}$ as a function of $W_{\gamma\gamma}$. The cross section was derived from the relationship:

$$N_{\omega\rho^0}=L_{e^+e^-}\,BR(\omega)\cdot\int_{W_{\gamma\gamma\min}}^{W_{\gamma\gamma\max}}A(W_{\gamma\gamma})\,\sigma_{\gamma\gamma\to\omega\rho^0}(W_{\gamma\gamma})\frac{dL^{TT}_{\gamma\gamma}(W_{\gamma\gamma})}{dW_{\gamma\gamma}}\,dW_{\gamma\gamma} \quad (2)$$

where $N_{\omega\rho^0}$ is the final number of reconstructed $\omega\rho^0$ events in the data, $BR(\omega)$ is the branching ratio $\omega\to\pi^+\pi^-\pi^0$, $L_{e^+e^-}$ is the integrated e^+e^- luminosity, $A(W_{\gamma\gamma})$ is the detector acceptance and $L_{\gamma\gamma}$ is the luminosity function. In this analysis the production of the $\omega\rho^0$ final state could be studied in the range $W_{\gamma\gamma}=1.2$–3.0 GeV.

In order to obtain the total number of ω mesons contained in the sample, the $\pi^+\pi^-\pi^0$ mass spectrum was fitted using a sum of distributions obtained from Monte Carlo events for the processes $\gamma\gamma\to\omega\rho^0$, $\gamma\gamma\to\omega\pi^+\pi^-$, $\gamma\gamma\to\pi^+\pi^-\pi^0\rho^0$ and $\gamma\gamma\to5\pi$. This fit yielded an ω signal containing 125 ± 16 entries (Fig. 3a). Figure 3b shows the recoil $\pi^+\pi^-$ mass spectrum for the accepted $\pi^+\pi^-\pi^0$ combinations. A similar fit yielded an estimate of about 210 entries in the ρ^0 signal.

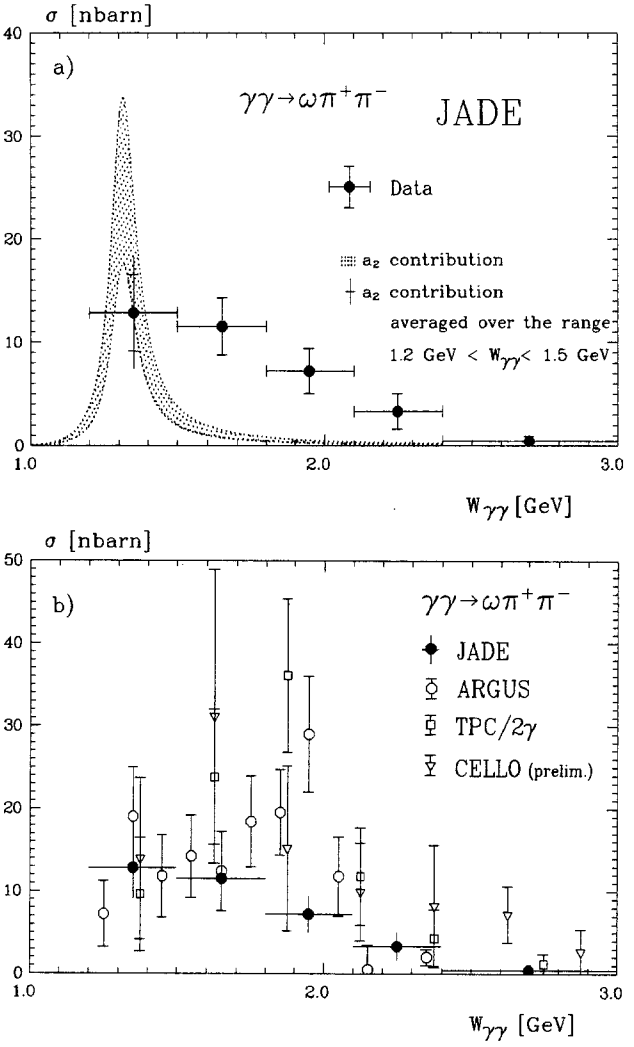

Fig. 4. a Cross section for $\gamma\gamma\to\omega\pi^+\pi^-$. The error bars are statistical only. Also shown is the expected $a_2(1320)$ contribution. **b** Comparison of measured cross sections for $\gamma\gamma\to\omega\pi^+\pi^-$

Table 1. Number of events with an ω meson and deduced cross sections in each $W_{\gamma\gamma}$ bin. Also quoted is the expected background from the reactions $\gamma\gamma\to\omega\omega$ and $\gamma\gamma\to\omega\pi^+\pi^-\pi^0$

$W_{\gamma\gamma}$ [GeV]	$A(W_{\gamma\gamma})\times BR_\omega$	$\int L^{TT}_{\gamma\gamma}\times L_{e^+e^-}$ [nbarn^{-1}]	$N_{\omega\pi^+\pi^-}$	N_ω background	Correction factor	$\sigma_{\gamma\gamma\to\omega\pi^+\pi^-}$ [nbarn]
1.2–1.5	0.0035	941	37.6 ± 8.8	4.7 ± 3.7		12.8 ± 3.7
1.5–1.8	0.0066	685	47.0 ± 9.0	6.7 ± 3.5		11.5 ± 2.8
1.8–2.1	0.0087	522	28.5 ± 7.4	3.0 ± 2.2	1.28	7.2 ± 2.2
2.1–2.4	0.0103	411	13.0 ± 5.6	2.0 ± 0.7		3.3 ± 1.7
2.4–3.0	0.0130	607	3.6 ± 3.0	0.9 ± 0.3		0.4 ± 0.5

For the determination of the $W_{\gamma\gamma}$ dependence of the cross section $\sigma_{\gamma\gamma\to\omega\rho^0}$, the $W_{\gamma\gamma}$ range was divided into five bins (Table 1). Since the ω meson is much easier to identify in invariant mass spectra than the broad ρ^0 meson, we first determined the number of events containing an ω meson and hence derived the inclusive cross section $\gamma\gamma\to\omega\pi^+\pi^-$. For this purpose the fit of the $\pi^+\pi^-\pi^0$ mass spectrum to the Monte Carlo distributions was repeated in each $W_{\gamma\gamma}$ bin. The expected background contribution from the reactions $\gamma\gamma\to\omega\omega$ and $\gamma\gamma\to\omega\pi^+\pi^-\pi^0$ was subtracted in each bin (Table 1). The resulting cross section is shown in Fig. 4, where the computed contribution from the reaction $\gamma\gamma\to a_2(1320)\to\omega\pi^+\pi^-$ is also plotted. The latter contribution was deduced from a weighted world average of the $\gamma\gamma$ width of the a_2 meson of 0.96 keV $\pm$ 0.09 keV [23] and a branching ratio into $\omega\pi^+\pi^-$ of 10.6% $\pm$ 3.2% [24]. The a_2 contribution can account for the whole measured cross section in the first $W_{\gamma\gamma}$ bin, but, due to the large errors on the branching ratio $a_2\to\omega\pi^+\pi^-$, there is room for contributions from other processes. In Fig. 4b the cross section is compared to the results from the ARGUS and TPC/2γ collaborations [25, 26] and to the preliminary results from the CELLO collaboration [27].

To determine the fraction of $\gamma\gamma\to\omega\pi^+\pi^-$ events, in which the $\pi^+\pi^-$ system originates from a ρ^0 decay, the correlation between the $\pi^+\pi^-\pi^0$ and $\pi^+\pi^-$ masses was investigated. In Fig. 5a, the correlation plot of the $\pi^+\pi^-\pi^0$ combinations against the $\pi^+\pi^-$ combinations is shown for $W_{\gamma\gamma}>1.55$ GeV, as are the projections onto the $\pi^+\pi^-\pi^0$ and $\pi^+\pi^-$ axes. Nearly all $\pi^+\pi^-\pi^0$ combination in the ω peak have a recoiling $\pi^+\pi^-$ mass in

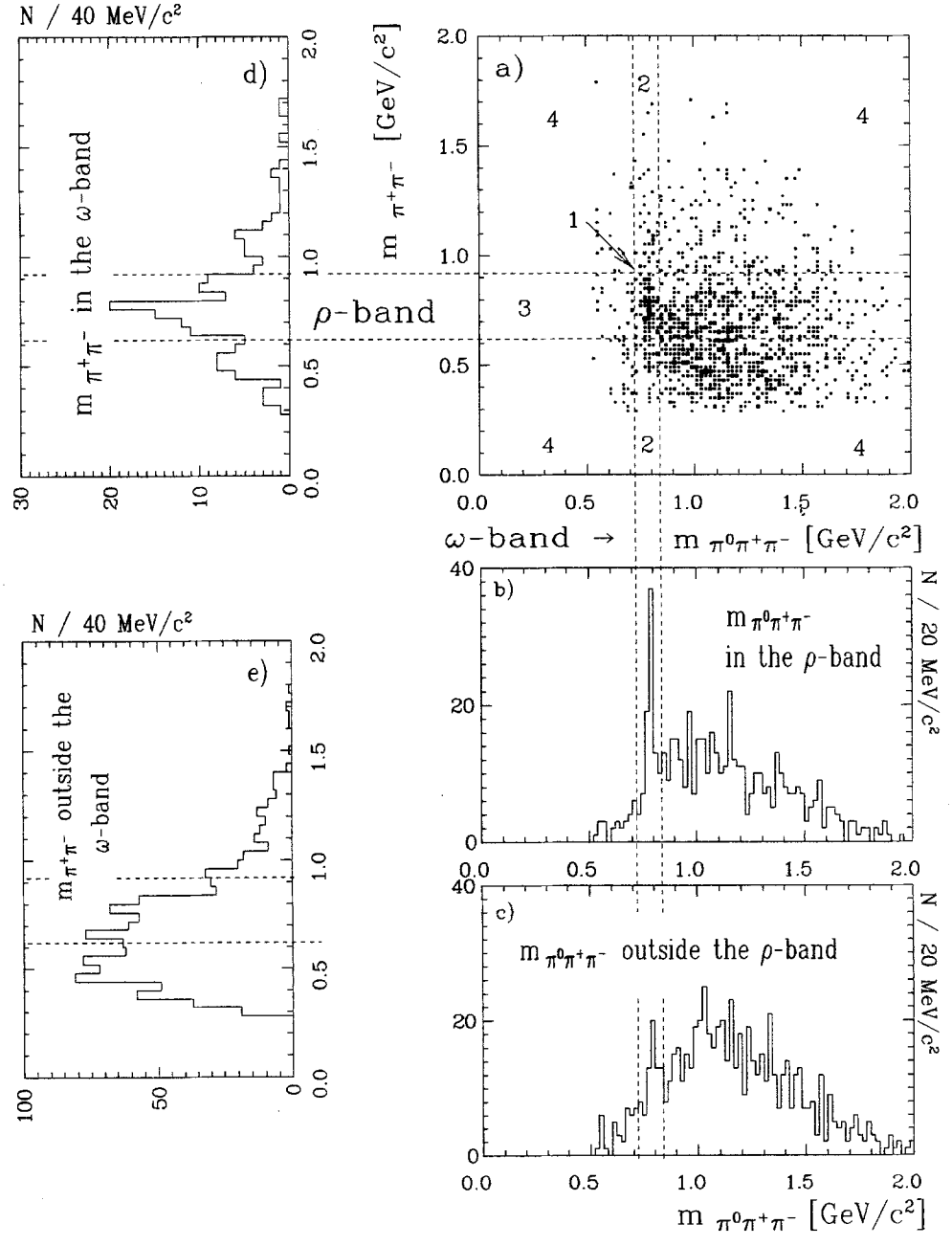

Fig. 5. a Correlation plot $m_{\pi^+\pi^-}$ against $m_{\pi^+\pi^-\pi^0}$ for $W_{\gamma\gamma}$ > 1.55 GeV. **b** and **c** Projections onto the $m_{\pi^+\pi^-\pi^0}$ axis. **d** and **e** Projections onto the $m_{\pi^+\pi^-}$ axis

Table 2. Result of correlation plot fit

$W_{\gamma\gamma}$ [GeV]	$f_{\omega\rho^0}$ in %	$f_{\omega\pi^+\pi^-}$ in %	$f_{\rho^0 3\pi}$ in %	$f_{5\pi}$ in %	N_{tot}	$n_{\omega\rho^0}/n$	$N_{\omega\rho^0}$	$\sigma_{\gamma\gamma\to\omega\rho^0}$ [nbarn]
1.2–1.5	–	–	–	–	–	–	–	–
1.5–1.8	65±15	0±17	35±12	0±12	221	0.28	40.2±9.3	11.5±2.9
1.8–2.1	20±10	10±11	4±19	66±20	320	0.28	18.8±9.8	5.1±2.6
2.1–2.4	14± 7	1± 7	70±28	15±30	297	0.29	12.1±6.0	3.7±1.8
2.4–3.0	4± 4	0± 4	43±27	53±27	270	0.34	3.7±3.7	0.6±0.6

the ρ^0 band (0.62–0.92 GeV/c^2) (Fig. 5b). Similarly the $\pi^+\pi^-$ mass recoiling from the $\pi^+\pi^-\pi^0$ combination in the ω (0.72–0.84 GeV/c^2) band exhibits an enhanced ρ^0 signal. This indicates that the $\gamma\gamma\to\omega\pi^+\pi^-$ data are dominated by $\omega\rho^0$ production.

In order to get a quantitative estimate of the number of $\omega\rho^0$ events, Monte Carlo distributions of various processes were fitted to the data using maximum likelihood techniques. The processes considered were $\omega\rho^0$ production, ω with non resonant $\pi^+\pi^-$ production, ρ^0 with non-resonant $\pi^+\pi^-\pi^0$ production and a $\pi^+\pi^-\pi^+\pi^-\pi^0$ state produced according to five body phase space. For this purpose the correlation plot was divided into four regions (Fig. 5a). The number of entries observed in region i was assumed to the Poisson distributed giving a probability P_i to observe N_i entries in region i:

$$P_i = \frac{e^{T_i} T_i^{N_i}}{N_i!} \tag{3}$$

where T_i is the "true" number of entries in region i, which in this model is composed of the following contributions:

$$T_i = (\alpha^i_{\omega\rho^0} f_{\omega\rho^0} + \alpha^i_{\omega\pi^+\pi^-} f_{\omega\pi^+\pi^-} + \alpha^i_{\rho^0 3\pi} f_{\rho^0 3\pi} + \alpha^i_{5\pi} f_{5\pi}) \cdot N_{\text{tot}} \tag{4}$$

The f_{xy}'s are the fraction of the total number of entries N_{tot} due to the process xy. The α_{xy}'s are the fraction of entries in the region i for the process xy. The parameters f_{xy} were constrained to the range 0–1. The product of the P_i forms the likelihood function, the logarithm of which was maximized by varying the parameters f_{xy}. After subtraction of the expected background from the reactions $\gamma\gamma\to\omega\omega$ and $\gamma\gamma\to\omega\pi^+\pi^-\pi^0$, the fit was performed separately in the different $W_{\gamma\gamma}$ regions, except for the lowest $W_{\gamma\gamma}$-bin, 1.2–1.5 GeV*.

In Table 2 the fitted fractions f_{xy} are shown together with the derived cross sections. The fractions are related to the number of entries in the correlation plot. To get the corresponding number of $\omega\rho^0$ events it is necessary to know the amount of the remaining combinatorial background, i.e. the relation of the correct $\pi^+\pi^-\pi^0$ combinations to all combinations. These relations $n_{\omega\rho^0}/n$ were inferred from Monte Carlo data and are quoted in Table 2.

The result confirms the conclusion stated above that $\omega\rho^0$ production dominates $\omega\pi^+\pi^-$ production. In Fig. 6a the cross section is shown and compared with

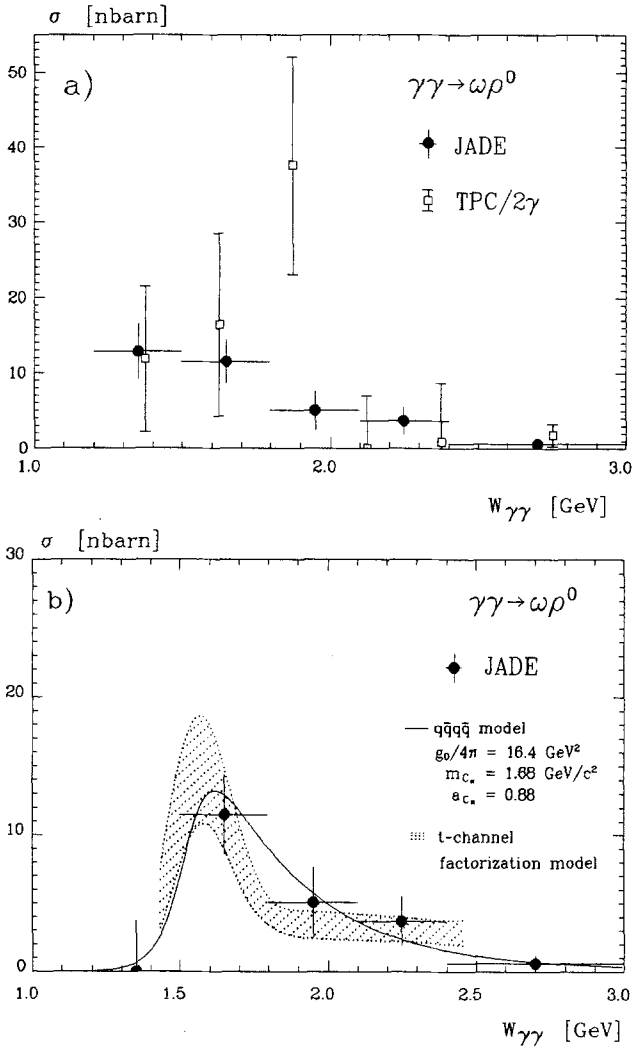

Fig. 6. a Cross section for $\gamma\gamma\to\omega\rho^0$ in comparison to the result of the TPC/2γ group. In the $W_{\gamma\gamma}$ range 1.2–1.5 GeV the inclusive cross section $\gamma\gamma\to\omega\pi^+\pi^-$ is plotted. The error bars are statistical only. **b** Comparison of the cross section of the $q\bar{q}q\bar{q}$ model and the t-channel factorization model. In the first $W_{\gamma\gamma}$ bin the cross section $\sigma_{\gamma\gamma\to\omega\pi^+\pi^-}$ is shown after subtraction of the expected contribution from the process $\gamma\gamma\to a_2(1320)\to\omega\pi^+\pi^-$

* This region is below the nominal threshold for $\omega\rho^0$ production. Due to the low statistics it was not possible to distinguish between the $\omega\pi^+\pi^-$ and $\omega\rho^0$ processes in this region. As mentioned above the expected contribution from the process $\gamma\gamma\to a_2(1320)\to\omega\pi^+\pi^-$ to the final state $\omega\pi^+\pi^-$ can account for the whole measured cross section $\gamma\gamma\to\omega\pi^+\pi^-$. Note that so far it is not clear whether the invariant mass of the $\pi^+\pi^-$ system from the a_2 decay can be described by a ρ^0 (below its nominal mass).

the results from the TPC/2γ group, who extracted the $\omega\rho^0$ fraction from their $\omega\pi^+\pi^-$ data using the same method.

In order to compare the measured cross section to the prediction of the $q\bar{q}q\bar{q}$ model [7–10] we have performed a fit in which the model parameters m_{C_π} (the mass of the $q\bar{q}q\bar{q}$ resonance) and a_{C_π} (used to account for non-calculable contributions) were varied while the dissociation coupling constant $g_0/4\pi$ was held fixed at 16.4 GeV^2 (corresponding to $Y=1.0$ GeV^2 in Eq. (2) in [8]). The mass obtained from the fit, 1.68 GeV/c^2, is near the predicted value of 1.65 GeV/c^2, while the a_{C_π} parameter, 0.88, is very high, indicating a considerable contribution from non-Zweig super-allowed decays (Fig. 6b). Also shown in Fig. 6b is the prediction of the t-channel factorization model [11–13]. It is seen that both models can be used to account for the measured $\gamma\gamma\to\omega\rho^0$ cross section.

Summary

The reaction $\gamma\gamma\to 2\pi^+ 2\pi^- \pi^0$ was studied using the JADE detector at the e^+e^- storage ring PETRA at DESY.

The cross section $\sigma_{\gamma\gamma\to\omega\pi^+\pi^-}$ was measured as a function of the total CMS energy of the $\gamma\gamma$-system, $W_{\gamma\gamma}$, in the range 1.2 GeV–3.0 GeV. The fraction of this cross section with intermediate ρ^0 production, i.e. the cross section $\sigma_{\gamma\gamma\to\omega\rho^0}$, was determined for $W_{\gamma\gamma}>1.5$ GeV. It was found that the inclusive cross section $\sigma_{\gamma\gamma\to\omega\pi^+\pi^-}$ is dominated by $\omega\rho^0$ production for $W_{\gamma\gamma}>1.5$ GeV. No enhancement was observed in the region around $W_{\gamma\gamma}=1.9$ GeV, in contrast to the results from the ARGUS and TPC/2γ collaborations.

Comparisons with the $q\bar{q}q\bar{q}$ model and the t-channel factorization model showed that both models are able to describe the measured cross section.

Acknowledgements. We are indebted to the PETRA machine group and the DESY computer centre staff for their excellent support during the experiment and to all the engineers and technicians of the collaborating institutions who have participated in the construction and maintenance of the apparatus. This experiment was supported by the Bundesministerium für Forschung und Technologie, by the Ministry of Education, Science and Culture of Japan, by the UK Science and Engineering Research Council through the Rutherford Appleton Laboratory and by the US Department of Energy. The visiting groups at DESY wish to thank the DESY directorate for the hospitality extended to them.

References

1. R. Brandelik et al.: Phys. Lett. 97B (1980) 448
2. M. Althoff et al.: Z. Phys. C – Particles and Fields 16 (1982) 13
3. PLUTO Coll. Ch. Berger et al.: DESY Preprint 87–173
4. CELLO Coll. H.J. Behrend et al.: Z. Phys. C – Particles and Fields 21 (1984) 205
5. H. Aihara et al.: Phys. Rev. D37 (1988) 28
6. JADE Coll.: reported by J. Olsson in the parallel session summarised by H. Spitzer; Proc. Vth Intern. Workshop on Photon-Photon Collisions. Aachen (1983) 45; Ch. Berger (ed.); Lecture Notes in Physics, Vol. 191, Berlin, Heidelberg, New York: Springer 1983; ARGUS Coll. H. Albrecht et al.: Phys. Lett. 217B (1989) 205; CELLO Coll. H.J. Behrend et al.: Phys. Lett. 218B (1989) 493
7. N.N. Achasov, S.A. Devyanin, G.N. Shestakov: Phys. Lett. 108B (1981) 134; Z. Phys. C – Particles and Fields 16 (1982) 55
8. N.N. Achasov, S.A. Devyanin, G.N. Shestakov: J. Nucl. Phys. (USSR) 32 (1984) 1098
9. B.A. Li, K.F. Liu: Phys. Lett. 118B (1982) 435; Phys. Rev. Lett. 51 (1983) 1510; Phys. Rev. D30 (1984) 613
10. K.F. Liu, B.A. Li: Phys. Rev. Lett. 58 (1987) 2288
11. G. Alexander, U. Maor, P.G. Williams: Phys. Rev. D26 (1982) 1198
12. G. Alexander, A. Levy, U. Maor: Z. Phys. C – Particles and Fields 30 (1986) 65
13. A. Levy: Proc. VIIth Intern. Workshop on Photon-Photon Collisions, Paris (1986). A. Courau, P. Kessler (eds.) p. 464, Singapore: World Scientific 1986
14. JADE Coll. W. Bartel et al.: Phys. Lett. 88B (1979) 171; Phys. Lett. 92B (1980) 206; Phys. Lett. 99B (1981) 277
15. S. Kawabata: Program write-up (1981), unpublished; S. Kawabata: Comput. Phys. Commun. 41 (1986) 127
16. G. Bonneau, M. Gourdin, F. Martin: Nucl. Phys. B54 (1973) 573
17. J.H. Friedman: J. of Comput. Phys. 7 (1971) 201; J.H. Friedman: Program write-up SAGE (1972), unpublished
18. J.D. Jackson: Nuovo Cimento 34 (1964) 1644
19. H. Messel, D.F. Crawford: Electron-photon shower distribution function. New York: Pergamon Press 1970; A. Sato: Master's Thesis, University of Tokyo (1978), unpublished; S. Yamada, J. Olsson: Jade Notes 20 and 20a, unpublished
20. R. Eichler: JADE-Note 65, unpublished
21. A. Wegner: Diplomarbeit, Hamburg University 1989, unpublished
22. ARGUS Coll. H. Albrecht et al.: Phys. Lett. 198B (1987) 2505
23. JADE Coll. T. Oest et al.: Z. Phys. C – Particles and Fields 47 (1990) 343
24. Particle Data Group: Phys. Lett. 204B (1988) 1
25. ARGUS Coll. H. Albrecht et al.: Phys. Lett. 196B (1987) 101
26. M.T. Ronan: Proc. VIIIth Intern. Workshop on Photon-Photon Collisions, Shoresh (1988); U. Karshon (ed.) p. 30, Singapore: World Scientific 1988; K.A. Derby: Ph.D. Thesis, University of California Berkeley (1987), unpublished
27. M. Feindt: Proc. VIIIth Intern. Workshop on Photon-Photon Collisions, Shoresh (1988); U. Karshon (ed.). p. 3, Singapore: World Sciencific 1988